

Actin Cortex Rearrangement Caused by Coupling with the Lipid Bilayer-Modeling Considerations

Ivana Pajic-Lijakovic · Milan Milivojevic

Received: 16 July 2014 / Accepted: 23 January 2015 / Published online: 7 February 2015
© Springer Science+Business Media New York 2015

Abstract Studies of cell membrane fluctuations under micro rheological measurements suggest that coupling between the lipid bilayer and the actin cortex can affect viscoelastic behavior of the single cell membranes. Coupling induces anomalous nature of energy dissipation during rearrangement of both: the actin cortex and the lipid bilayer. The actin cortex ability to rearrange for various cell types: erythrocytes, Jurkat cells, fibroblasts, epithelial lung cells, and muscle cells based on experimental data for storage and loss moduli versus angular velocity are considered. The cortex of softer cells such as erythrocytes, Jurkat cells, and fibroblasts has the ability to rearrange at low angular velocities which is quantified by their rearrangement time and the average size of the cortex micro domains. The rearrangement time of the cortex for Jurkat cells and fibroblasts is at the order of magnitude higher than that for erythrocytes, i.e., 2.70–7.53 s. The average size of the cortex micro domains for erythrocytes varied from 3.0 to 5.3 μm , for Jurkat cells is ~ 0.20 – $0.22 \mu\text{m}$ and for fibroblasts is $\sim 36 \text{ nm}$. Lower size of the micro domains and higher rearrangement time indicate the stiffer cortex structure. The cortex rearrangement for stiffer cells such as epithelial lung cells and muscle cells has never been observed.

Keywords Coupling of the actin cortex with the lipid bilayer · Mobility of actin filaments · The cortex ability to rearrange · The cell membrane · Modeling

Introduction

Mechanical properties of single living cells vary significantly depending on their function within organisms. Cell functions as adhesion, migration, and division are known to depend on deformability of the cell membrane (Mofrad et al. 2006). Significant attempts have been made to develop various micro rheological techniques for examination of the cell membrane viscoelasticity (Fabry et al. 2001; Alcaraz et al. 2003; Popescu et al. 2007; Amin et al. 2007; Puig-de-Morales-Marinkovic et al. 2007; Warren et al. 2013). However, little is reported about the structural changes of the actin cortex caused by coupling with the lipid bilayer. Rheological behavior of the cortex as: (1) fluidity, (2) homogeneity, (3) ability to rearrange could be estimated from experimental data sets of storage and loss moduli versus angular velocity.

Cell membrane is considered as a composite of the lipid bilayer and the actin cortex attached to the bilayer. However, the cortical actin network is also coupled to the intracellular cytoskeleton. The actin cortex is composed of stiff filaments of actin and actin-binding proteins (ABP) (Mofrad et al. 2006; Dalhaimer et al. 2007). The role of various ABP in mechanical behavior of the cortex for various cells has been unknown up to now. ABP vary (1) in type of actin-binding affinity caused by specific binding domains used and (2) in structure, number, and organization of their spacing rod domains (Wagner et al. 2006). Short cross-linkers, such as plastrin or fascin are classified as bundling proteins. Longer cross-linkers, such as α -actinin, filamin, and spectrin induce formation of isotropic network. Erythrocyte spectrin is included in the actin cortex formation. However, the role of non erythrocyte spectrin is quite different. Mangeat and Burrige (1984) reported that intracellular fibroblast spectrin don't affect

I. Pajic-Lijakovic (✉) · M. Milivojevic
Faculty of Technology and Metallurgy, University of Belgrade,
Karnegijeva 4, 11120 Belgrade, Serbia
e-mail: iva@tmf.bg.ac.rs

M. Milivojevic
e-mail: mmilan@tmf.bg.ac.rs

the integrity of the major actin-containing structures. The parameters are: (1) flexibility and length of ABP (2) length of stiff actin filaments, (3) concentration of actin filaments, (4) actin network mesh size, (5) network rearrangement and homogeneity, and (6) cortex thickness mainly influence rheological behavior of the cortex as well as cell stiffness. Flexible and long spectrin chains are key factors which determine erythrocyte elasticity. The actin network mesh size varies from 80 to 100 nm for erythrocytes (Gov 2007) to 15–30 nm for T cells (Dustin and Davis 2014) or less for stiffer cell type. The cortex thickness varies from ~ 2 nm for erythrocytes (Peng and Zhu 2013) to 5 nm–2 μm for contractile actin networks (Charras et al. 2006). Thickness of the apical membrane of human umbilical vein endothelial cells cortex is ~ 0.5 μm (Feneberg et al. 2004) while thickness of the fibroblasts cortex is ~ 0.1 μm (Bausch et al. 1998). The cortex stiffness could be estimated from the values of the surface shear modulus. Higher value of the surface shear modulus corresponds to the stiffer cortex. Consequently, the surface shear modulus of the apical membrane of human umbilical vein endothelial cells cortex is $\mu_{\text{SC}} = 2.5 \times 10^{-4}$ Pam (Feneberg et al. 2004) while for the fibroblast cortex is $\mu_{\text{SC}} = 2\text{--}4 \times 10^{-3}$ Pam (Bausch et al. 1998). In comparison, the surface shear modulus of the erythrocyte cortex is the lowest $\mu_{\text{SC}} = 5.7 \times 10^{-6}$ Pam (Peng and Zhu 2013) indicating the most elastic structure. The average radius of gyration of the ABP could be calculated from the values of the surface shear modulus as $\langle r_{\text{g}}^2 \rangle = \frac{kT}{\mu_{\text{SC}}}$ (where $\langle r_{\text{g}}^2 \rangle$ is the square of average radius of gyration, k is Boltzmann constant, and T is temperature) (Gov 2007). The average radius of gyration of spectrin chains in erythrocytes is ~ 45 nm (Gov 2007), while the corresponding average radius of gyration of cross linking protein in fibroblasts is much lower and equal to $\sim 1\text{--}1.4$ nm. Length of actin filaments varies from ~ 40 nm in the erythrocyte cortex to ~ 1 μm in the muscle cortex (Almenar-Queralt et al. 1999).

Dalhaimer et al. (2007) considered three types of the actin network depending on actin to cross linker length ratio: loose, semi-loose, and tight networks. The lipid bilayer is structurally inhomogeneous and consists of lipid rafts (Mikhalyov and Samsonov 2011). Homogeneity of the actin network depends on: actin concentration, length, and elasticity of ABP. Borukhov et al. (2005) considered the rearrangement of the actin cortex into: isotropic, nematic, cubatic, and bundle network types. They proposed the actin–actin interaction potential as: (1) hard core repulsion dominates at short distances, (2) ABP mediates attractions presented at intermediate range, and (3) screened electrostatic repulsions compete with the ABP-mediated attractions at long distances. The erythrocyte spectrin–actin network has been treated as ensembles of the

micro domains of different sizes (Pradhan et al. 2004; Pajic-Lijakovic and Milivojevic 2014). Cell softness mainly affected by structural organization of the actin network could be quantified by the value of the Young's modulus. Higher values of the Young's modulus correspond to the stiffer cortex structure. The values of Young's modulus for various cell types are different in many order of magnitude. Young's modulus for muscle cells is $E_{\text{c}} = 10\text{--}45$ kPa while fibroblasts are more elastic with Young's modulus equal to $E_{\text{c}} = 4\text{--}5$ kPa (Kuznetsova et al. 2007). Young's modulus of lung epithelial cells is the same order of magnitude as for fibroblasts and equal to $E_{\text{c}} = 3.26$ kPa (Wagh et al. 2008). In cancer cells, the Young's modulus is less than 0.1 kPa. Young's modulus of Jurkat cells is $E_{\text{c}} = 0.02\text{--}0.08$ kPa (Kuznetsova et al. 2007). Cai et al. (2010) reported that Jurkat cells are more elastic than lymphocytes. They determined that Young's modulus for Jurkat cells is $E_{\text{c}} = 0.51 \pm 0.06$ kPa and for lymphocytes equals to $E_{\text{c}} = 1.24 \pm 0.09$ kPa.

Membrane deformation rate leads to viscoelastic behavior. Unlike the actin cortex which behaves viscoelastically (Mofrad et al. 2006), rheological response of the lipid bilayer is purely dissipative as reported by Harland et al. (2011). We have proposed a 3D constitutive model for describing viscoelasticity of the erythrocyte membrane based on micro rheological measurements (Pajic-Lijakovic and Milivojevic 2014). Herein, this model is expanded and together with the model proposed by Djordjevic et al. (2003) applied for viscoelasticity modeling of the cell membranes for various cell types: Jurkat cells, fibroblasts, epithelial lung cells, and muscle cells. This analysis is based on experimental data obtained by Fabry et al. (2001), Alcaraz et al. (2003), Jonas et al. (2006), Popescu et al. (2007), Amin et al. (2007), Puig-de-Morales-Marinkovic et al. (2007), Warren et al. (2013).

Theory

Experimental data for the storage and loss moduli of the cell membranes as a function of angular velocity, presented in Amin et al. (2007), Puig-de-Morales-Marinkovic et al. (2007), and Popescu et al. (2007) for erythrocytes are estimated and compared with the data for the storage and loss moduli, presented in Fabry et al. (2001), Alcaraz et al. (2003), Jonas et al. (2006), and Warren et al. (2013) for various cell types. The data shows three important characteristics:

- (1) Scaling of storage and loss moduli versus angular velocity shows anomalous nature of energy dissipation during the membrane fluctuations that can be described by fractional derivatives (Podlubny 1999).

- (2) Ratio $\frac{G'}{G''}(\omega)$ (where G' is storage modulus and G'' is loss modulus) could be higher, lower, and equal to one dependent on angular velocity and cell type. When $\frac{G'}{G''}(\omega) > 1$ suggests presence of viscoelastic solid, while the ratio $\frac{G'}{G''}(\omega) < 1$ indicates presence of viscoelastic liquid. The ratio could be equal to one at critical angular velocity ω_c , i.e., $\frac{G'}{G''}(\omega_c) = 1$. These rheological behaviors for various cell type and angular velocity range $\omega \in [\omega_0, \omega_\infty]$ (where ω_0 and ω_∞ are the initial and final values of the angular velocity) is shown in Table 1.
- (3) Softer cells such as erythrocytes, Jurkat cells, and fibroblasts show rapid non-linear increase of the storage and loss moduli at low angular velocities while the same behavior has not been observed for stiffer cells such as lung and muscle cells. For softer cells, two regimes could be established based on the experimental data. Regime 1 for low angular velocities corresponds to $\omega \in [\omega_0, \omega^*]$ (where ω^* is the threshold angular velocity) and therefore longer relaxation times $t \in [t^*, t_{\max}]$ (where $t^* = \frac{2\pi}{\omega^*}$ is the characteristic time and $t_{\max} = \frac{2\pi}{\omega_0}$ is the maximum relaxation time). For example, ω^* for erythrocytes has been estimated as $30 \frac{\text{rad}}{\text{s}}$ (Pajic-Lijakovic and Milivojevic 2014). Longer relaxation times ensure rearrangement of the actin cortex within the micro domains. In contrast to this behavior, in regime 2 storage and loss moduli increase more slowly for high angular velocities ($\omega > \omega^*$), which indicates to shorter relaxation times $t \in [t_{\min}, t^*]$ (where $t_{\min} =$

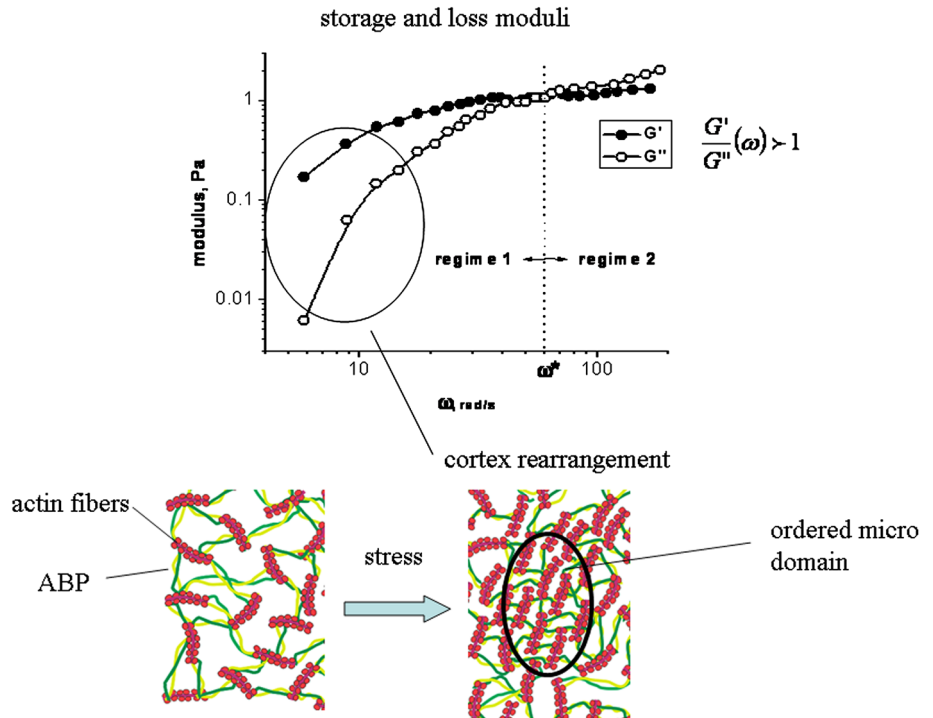
$\frac{2\pi}{\omega_\infty}$ is the minimum relaxation time). Short relaxation times in regime 2 ensure only conformational changes of parts of protein chains within the cortex. We consider the ability of the actin cortex to rearrange for various cell types from rheological stand point by formulating the corresponding constitutive modeling equation.

The experimental conditions: (1) $\frac{G'}{G''}(\omega) > 1$ and (2) rapid non-linear increase of both storage and loss moduli observed at low angular velocities for softer cells are related with the actin cortex ability to rearrange. Changes of the actin local density during the cortex-bilayer coupling influence molecular interactions. In the actin cortex, electrostatic repulsion between the actin filaments and ABP favor large-angle crossings between filaments. However, steric repulsions are minimized and ABP binding is maximized when the filaments are parallel. These effects favor parallel orientation specific for nematic ordering. Consequently, local increase of the actin density could induce phase transition of the actin cortex from isotropic to nematic (Borukhov et al. 2005). The course-consequence relation of the cortex stiffening obtained from storage and loss moduli versus angular velocity on one hand and the disorder to the order phase transition of actin filaments on the other hand is presented in Fig. 1. The actin cortex is the softest at low angular velocity due to the presence of the ordered micro domains. Dalhaimer et al. (2007) reported that “soft elasticity” of nematic network arises from broken rotational symmetry and has been described as “liquid crystal elastomer”. An increase of angular velocity causes actin

Table 1 Rheological behavior of various cell types

	$\omega_0 \left(\frac{\text{rad}}{\text{s}}\right)$	$\omega_{c1} \left(\frac{\text{rad}}{\text{s}}\right)$	$\omega \leq \omega_{c1}$	$\omega_{c1} < \omega \leq \omega_{c2}$	$\omega > \omega_{c2}$
	$\omega_\infty \left(\frac{\text{rad}}{\text{s}}\right)$	$\omega_{c2} \left(\frac{\text{rad}}{\text{s}}\right)$	$\frac{G'}{G''} < 1$	$\frac{G'}{G''} > 1$	$\frac{G'}{G''} < 1$
Erythrocytes (Amin et al. 2007)	8	–	No	Yes	Yes
	6.0×10^2	5.0×10^2			
Erythrocytes (Popescu et al. 2007)	6	–	No	Yes	Yes
	2.0×10^2	1.5×10^2			
Erythrocytes (Puig-de-Morales-Marinkovic et al. 2007)	7	–	No	Yes	Yes
	6.0×10^2	2.0×10^2			
Fibroblasts (Jonas et al. 2006)	1.4	10	Yes	Yes	Yes
	1.0×10^5	3.0×10^4			
Jurkat cells (Warren et al. 2013)	0.4	–	No	Yes	Yes
	5.4×10^2	2.0×10^2			
Lung cells (Alcaraz et al. 2003)	0.8	–	No	Yes	Yes
	8.0×10^2	8.0×10^2			
Muscle cells (Fabry et al. 2001)	0.05	–	No	Yes	Yes
	8.0×10^3	2.0×10^3			

Fig. 1 Schematic representation of the membrane non-linear stiffening at low angular velocities is related with the actin cortex rearrangement within micro domains



disordering. Actin disordering and conformational changes of ABP which represent worm like chains induce the cortex non-linear stiffening pronounced for softer cells.

Development of the constitutive equation includes combining of the rheological elements: spring, spring pot, dashpot, and Eyring’s element. Eyring’s element has been formulated by Pajic-Lijakovic and Milivojevic (2014) for describing the long-time cortex rearrangement (regime 1). Lamellar structure made by the lipid bilayer attached at the actin cortex under micro rheological measurement conditions indicates their parallel combination. For this case, the stress within the membrane satisfies the condition:

$$\begin{aligned} \tilde{\sigma}(t) &= \left(\sum_j^n \tilde{\sigma}_j(t) \right)_C + \left(\sum_l^m \tilde{\sigma}_l(t) \right)_L \text{ and } \tilde{\varepsilon}_1(t) = \tilde{\varepsilon}_j(t) \\ &= \dots = \tilde{\varepsilon}_n(t) = \tilde{\varepsilon}(t), \end{aligned} \tag{1}$$

where $\tilde{\sigma}(t)$ is the total stress, $\tilde{\sigma}_j(t)$ and $\tilde{\varepsilon}_j(t)$ is the stress and the strain for the corresponding rheological element, n and m are the number of the elements necessary for describing rheological behavior of the cortex and the lipid bilayer, respectively, the notation “C” and “L” are the cortex and the bilayer. Every rheological element describes the nature of energy storage and energy dissipation during the membrane structural ordering. It should be related to the multi scale interactions during the cortex-bilayer coupling.

Viscoelasticity of the cortex has been described by various fractional Kelvin-Voigt equations (Djordjevic et al. 2003; Mofrad et al. 2006; Pajic-Lijakovic and Milivojevic 2014). For the softer cells such as erythrocytes, the cortex

rheological behavior has been formulated separately for two regimes (Pajic-Lijakovic and Milivojevic 2014):

$$\begin{aligned} \tilde{\sigma}_C(t) &= \tilde{\sigma}_{\text{EyringC}}(t) + \tilde{\sigma}_{\text{spring potC}}(t) \text{ for regime 1,} \\ \tilde{\sigma}_C(t) &= \tilde{\sigma}_{\text{springC}}(t) + \tilde{\sigma}_{\text{spring potC}}(t) \text{ for regime 2,} \end{aligned} \tag{2}$$

where $\tilde{\sigma}_C(t)$ is the cortex stress, $\tilde{\sigma}_{\text{springC}}(t)$, $\tilde{\sigma}_{\text{EyringC}}(t)$ and $\tilde{\sigma}_{\text{spring potC}}(t)$ are the stresses tensor parts for spring, Eyring’s element and spring pot.

For the stiffer cells such as lung cells and muscle cells, the rheological regimes are not distinguishes. The corresponding cortex rheological behavior is formulated for the whole range of the relaxation times (Djordjevic et al. 2003):

$$\tilde{\sigma}_C(t) = \tilde{\sigma}_{\text{springC}}(t) + \tilde{\sigma}_{\text{spring potC}}(t) + \tilde{\sigma}_{\text{dashpotC}}(t), \tag{3}$$

where $\tilde{\sigma}_{\text{dashpotC}}(t)$ is the stress tensor parts for dashpot. The stress within the lipid bilayer is primarily affected by its fluidity (Harland et al. 2011) with anomalous nature of energy dissipation and has been described by a spring pot (Pajic-Lijakovic and Milivojevic 2014):

$$\tilde{\sigma}_L(t) = \tilde{\sigma}_{\text{spring potL}}(t), \tag{4}$$

where the $\tilde{\sigma}_{\text{spring potL}}(t)$ is the stress for spring pot which describe the lipid bilayer rheological behavior. The lipid bilayer stress is the same order of magnitude as the cortex stress for softer cells $\tilde{\sigma}_L(t) \approx \tilde{\sigma}_C(t)$. For stiffer cells, the cortex stress is much higher than the lipid bilayer stress $\tilde{\sigma}_L(t) \ll \tilde{\sigma}_C(t)$. Spring quantifies purely reversible, elastic nature of the cortex structural rearrangement. It could

describe the part of cortex structural changes primarily caused by covalent bonds loading under stress.

The stress–strain relation for the cortex spring is:

$$\tilde{\sigma}_{\text{springC}}(t) = G_{\text{SC}} \tilde{\varepsilon}(t), \quad (5)$$

where G_{SC} is the 3D shear modulus of the cortex equal to $G_{\text{SC}} = \frac{kT}{\langle \xi_d^2 \rangle h_c}$, $\langle \xi_d^2 \rangle$ is the characteristic size of the cortex, h_c is the cortex thickness. When $\langle \xi_d^2 \rangle \rightarrow \xi_m^2$ (where ξ_m is the mesh size), the cortex is homogeneous. On the other side, the condition $\langle \xi_d^2 \rangle \gg \xi_m^2$ indicates the micro domain formation as a measure of the cortex in-homogeneity. Elastic response of the cortex constituents is characteristic of the short time dynamics (i.e., higher angular velocities regime).

Dashpot quantifies purely irreversible, viscous nature of the structural rearrangement. The stress–strain relation for the cortex dashpot is:

$$\tilde{\sigma}_{\text{dashpotC}}(t) = \eta_C D_t^1 \tilde{\varepsilon}(t), \quad (6)$$

where η_C is the 3D cortex viscosity and $D_t^1 = \frac{d}{dt}$. Purely irreversible response of the cortex could be dominant for short time dynamics (i.e., higher angular velocities) especially for the stiffer cortex structure.

Structural changes which induce anomalous nature of energy dissipation could be quantified by the spring pot. Anomalous nature of energy dissipation is described by the fractional derivatives (Podlubny 1999). The stress–strain relation for the cortex spring pot is:

$$\tilde{\sigma}_{\text{spring potC}}(t) = \eta_{\text{effC}} D_t^\alpha \tilde{\varepsilon}(t), \quad (7)$$

where η_{effC} is the cortex effective modulus, $D_t^\alpha (\bullet)$ is the fractional derivative and α is the order of the fractional derivative such that $0 < \alpha < 1$. Caputo's definition of the fractional derivative of some function $f(t)$ is given as follows: $D_t^\alpha (f(t)) = \frac{1}{\Gamma(1-\alpha)} \frac{d}{dt} \int_0^t \frac{f(t')^{(1)}}{(t-t')^\alpha} dt'$ (where $\Gamma(1-\alpha)$ is the gamma function). When $\alpha \rightarrow 1$, the spring pot becomes the dashpot and the effective modulus η_{effC} becomes the 3D viscosity η_C . On the other side, when $\alpha \rightarrow 0$, the spring pot becomes the spring and the effective modulus η_{effC} becomes the 3D shear modulus G_{SC} . The anomalous nature of energy dissipation quantified by the spring pot corresponds to breaking of some secondary bonds within the cortex. This type of the response could be characteristic of short and long-time dynamics (i.e., whole range of angular velocities) pronounced for the softer cortex structure. Pajic-Lijakovic and Milivojevic (2014) obtained for erythrocytes that spring pots for the lipid bilayer is equal to:

$$\tilde{\sigma}_{\text{spring potL}}(t) = \eta_{\text{effL}} D_t^{2\alpha} \tilde{\varepsilon}(t), \quad (8)$$

where η_{effL} is the effective modulus of the lipid bilayer. This important result points to the nature of energy

dissipation during the erythrocyte cortex-bilayer coupling expressed as: $\tilde{\sigma}_{\text{spring potL}}(t) \sim D_t^{2\alpha} \tilde{\sigma}_{\text{spring potC}}(t)$. In this context, it would be interesting to consider the cortex-bilayer coupling for other softer cell types.

Long-time structural rearrangement (i.e., lower angular velocity regime) induces anomalous nature of energy dissipation during conformational changes of ABP chains which influences the actin filaments mobility. It has been quantified by the cortex Eyring's element (Pajic-Lijakovic and Milivojevic 2014). The stress–strain relation for the Eyring element is:

$$\tilde{\sigma}_{\text{EyringC}}(t) = B D_t^{-(\alpha+1)} \tilde{\varepsilon}(t), \quad (9)$$

where B is the cortex rearrangement modulus and $1 + \alpha$ is the order of the fractional derivative. The order of the fractional derivative in the range $1 < (\alpha + 1) < 2$, ensures non-linear stiffening of the cortex with angular velocity increase obtained for softer cells (Fig. 1). The rearrangement modulus is equal to $B = \frac{G_s}{\tau^{(\alpha+1)}}$, τ is the rearrangement time of the ordered micro domains equal to $\tau = \left[f \left(e^{-\frac{\Delta G - E'}{kT}} - e^{-\frac{\Delta G + E'}{kT}} \right) \right]^{-1}$, f is characteristic frequency, ΔG is Gibbs energy barrier, E' is energy perturbation equal to $E' \approx kT$, k is Boltzmann constant, and T is temperature, $f e^{-\frac{\Delta G - E'}{kT}}$ is the probability of the rearrangement in the direction of the stress and $f e^{-\frac{\Delta G + E'}{kT}}$ is the probability of the rearrangement in the opposite direction. The Gibbs energy barrier for the loose network such as the soft erythrocyte spectrin–actin cortex is the same order of magnitude as the energy perturbation E' (approximately equal to $\Delta G \approx 2 - 3 kT$) (Pajic-Lijakovic and Milivojevic 2014). The value of ΔG represents the key parameter which describe the cortex ability to rearrange. For the actin cortex in various cell types, ΔG value depends on $\frac{L_A}{L_X}$ and $\frac{L_{pX}}{L_X}$ (where L_A is the actin filament length, L_X is the ABP length, and L_{pX} is the ABP persistence length). It can be expressed as $\Delta G \sim \left(\frac{L_A}{L_X} \right) \left(\frac{L_{pX}}{L_X} \right)$. For tight network $\frac{L_A}{L_X} \gg 1$ (Dalhaimer et al. 2007), the energy barrier is $\Delta G \gg E'$. For this case, the cortex rearrangement under thermal fluctuations is not possible.

The constitutive model Eq. 1 should be transformed using the Fourier integral transform. The transforming equation is $F[\tilde{\sigma}_j(t)] = G_j * F[\tilde{\varepsilon}(t)]$ (where $F[\circ]$ is the Fourier operator and G_j^* is the complex dynamic modulus for the corresponding rheological element j equal to $G_j^* = G_j' + iG_j''$ and $i = \sqrt{-1}$, G_j' is the storage modulus and G_j'' is the loss modulus). The storage modulus quantifies storage energy within the system while the loss modulus quantifies dissipated energy during the rearrangement. The complex dynamical modulus for the membrane is equal to

$G^* = \left(\sum_j^n G_j^*\right)_C + \left(\sum_j^m G_j^*\right)_L$. Fourier transform of the fractional derivative of the strain $\tilde{\varepsilon}(t)$ is expressed as $F[D_t^\alpha(\tilde{\varepsilon}(t))] = (i\omega)^\alpha F[\tilde{\varepsilon}(t)]$ (where ω is angular velocity). The corresponding expressions of the storage modulus for softer cells within both regimes are:

$$\begin{aligned} G'(\omega) &= -B \frac{1}{\omega^{\alpha+1}} \sin\left(\frac{\pi\alpha}{2}\right) + \eta_{\text{eff}C_1} \omega^\alpha \cos\left(\frac{\pi\alpha}{2}\right) \\ &\quad - \eta_{\text{eff}L} \omega^{2\alpha} \left(1 - 2 \cos^2\left(\frac{\pi\alpha}{2}\right)\right) \text{ for regime 1} \\ G'(\omega) &= G_{\text{s}C} + \eta_{\text{eff}C_1} \omega^\alpha \cos\left(\frac{\pi\alpha}{2}\right) \\ &\quad - \eta_{\text{eff}L} \omega^{2\alpha} \left(1 - 2 \cos^2\left(\frac{\pi\alpha}{2}\right)\right) \text{ for regime 2.} \end{aligned} \quad (10)$$

The loss modulus is:

$$\begin{aligned} G''(\omega) &= -B \frac{1}{\omega^{\alpha+1}} \cos\left(\frac{\pi\alpha}{2}\right) + \eta_{\text{eff}C} \omega^\alpha \sin\left(\frac{\pi\alpha}{2}\right) \\ &\quad + \eta_{\text{eff}L} \omega^{2\alpha} 2 \sin\left(\frac{\pi\alpha}{2}\right) \cos\left(\frac{\pi\alpha}{2}\right) \text{ for regime 1} \\ G''(\omega) &= \eta_{\text{eff}C} \omega^\alpha \sin\left(\frac{\pi\alpha}{2}\right) \\ &\quad + \eta_{\text{eff}L} \omega^{2\alpha} 2 \sin\left(\frac{\pi\alpha}{2}\right) \cos\left(\frac{\pi\alpha}{2}\right) \text{ for regime 2.} \end{aligned} \quad (11)$$

The five model parameters τ , $\eta_{\text{eff}C}$, $\eta_{\text{eff}L}$, $G_{\text{s}C}$, and α were obtained by independent comparative analyses of the four experimental data sets $G'(\omega)$ versus ω and $G''(\omega)$ versus ω for regimes 1 and 2 and model predictions (Eqs. 10–11). The corresponding expressions of the storage and loss moduli for stiffer cells within the whole range of angular velocities are:

$$\begin{aligned} G'(\omega) &= G_{\text{s}C} + \eta_{\text{eff}C} \omega^\alpha \cos\left(\frac{\pi\alpha}{2}\right) \\ G''(\omega) &= \eta_{\text{eff}C} \omega^\alpha \sin\left(\frac{\pi\alpha}{2}\right) + \eta_C \omega \end{aligned} \quad (12)$$

The four model parameters: $\eta_{\text{eff}C}$, η_C , $G_{\text{s}C}$, and α were obtained by independent comparative analyses of the two experimental data sets $G'(\omega)$ versus ω and $G''(\omega)$ versus ω for whole range of angular velocities. Constitutive model for softer cells (Eqs. 10–11) needs five model parameters while for stiffer cells (Eq. 12) needs four model parameters. However, the five parameters were obtained by independent comparative analysis of the four experimental data sets for regimes 1 and 2, while the four parameters were obtained by comparative analysis of the two experimental data sets for whole range of angular velocities. The calculated values were fitted with the experimental data by minimizing the squared magnitude of the residuals of the storage and loss moduli in order to determine the optimal values of the model parameters.

The comparative analysis of constitutive model equations for softer and stiffer cell types points that: (1) the cortex response to the stress for stiffer cells offers additional energy dissipation quantified by dashpot and (2) the cortex rearrangement at low angular velocities has not been observed for stiffer cells due to less mobility of actin filaments. Decrease of actin mobility induces increase of the energetic barrier ΔG to the actin structural ordering in the direction of stress. Consequently, energetic perturbations of the actin cortex caused by coupling with the lipid bilayer are not enough for the cortex rearrangements.

Results and Discussions

Model considerations of the storage and loss moduli for erythrocytes, Jurkat cells, fibroblasts, epithelial lung cells, and muscle cells indicate anomalous nature of energy dissipation caused by coupling between the bilayer and the actin cortex. Experimental data (Fabry et al. 2001; Alcaraz et al. 2003; Jonas et al. 2006; Warren et al. 2013) were compared with the model predictions using Eqs. 10–11 for softer cells and 12 for stiffer cells. Experimental data and model prediction for erythrocytes has been reported by Pajic-Lijakovic and Milivojevic (2014). The corresponding values of the model parameters for comparison with the values determined for other cell types are shown in Table 2.

The storage and loss moduli vs. angular velocity for Jurkat cells under iso-osmotic and hypo-osmotic conditions (after $t_c = 2, 7, 12, 18, 23,$ and 28 min in hypo-osmotic solution, where t_c is cell-solution contact time) reported by Warren et al. (2013) were considered within two regimes (Eqs. 10–11). The estimated threshold angular velocity between the regimes ω^* for Jurkat cells is about $10 \frac{\text{rad}}{\text{s}}$. All experimental data shows similar functional trend. One representative data set for iso-osmotic condition is shown in Fig. 2. The model correlated with the experimental data with the standard deviation $\text{SD} = 0.0249 \pm 0.013$ for the storage modulus and $\text{SD} = 0.0326 \pm 0.010$ for the loss modulus for all data sets. Higher values of the storage and loss moduli for the same angular velocities were obtained for Jurkat cells (Warren et al. 2013) in comparison to those previously reported for erythrocytes (Pajic-Lijakovic and Milivojevic 2014) under iso-osmotic condition. It is noteworthy to estimate changes of the storage and loss moduli of Jurkat cells under hypo-osmotic conditions relative to iso-osmotic condition. Hypo-osmotic conditions induce cell shape changes, cell volume increase which leads to significant structural changes of the cell membrane. Higher values of the storage and loss moduli for the same angular velocities were obtained for Jurkat cells under hypo-

Table 2 Model parameters for various cell types

	G_{sC} (Pa)	η_{effC} (Pas ^α)	η_C (Pas)	η_{effL} (Pas ^{2α})	$\alpha(-)$	τ (s)
Erythrocytes (Amin et al. 2007; Pajic-Lijakovic and Milivojevic 2014)	0.08 ± 0.02	0.022 ± 0.001	–	0.01 ± 0.001	0.37 ± 0.01	0.12 ± 0.01
Erythrocytes (Popescu et al. 2007; Pajic-Lijakovic and Milivojevic 2014)	0.2 ± 0.1	0.15 ± 0.02	–	0.01 ± 0.001	0.38 ± 0.01	0.10 ± 0.01
Erythrocytes (Puig-de-Morales-Marinkovic et al. 2007; Pajic-Lijakovic and Milivojevic 2014)	0.07 ± 0.001	0.023 ± 0.001	–	0.01 ± 0.001	0.46 ± 0.01	0.36 ± 0.01
Jurkat cells (Warren et al. 2013) iso-osmotic	0.8 ± 0.1	R1: 1.2 ± 0.1 R2: 0.23 ± 0.02	–	0.008 ± 0.001	R1: 0.14 ± 0.01 R2: 0.43 ± 0.01	7.53 ± 0.2
Jurkat cells (Warren et al. 2013) hypo-osmotic	0.8 ± 0.1	R1: 1.2 ± 0.1 R2: 0.23 ± 0.02	–	0.008 ± 0.001	R1: 0.16 ± 0.01 R2: 0.43 ± 0.01	7.53 ± 0.2
$t_c = 2$ min						
Jurkat cells (Warren et al. 2013) hypo-osmotic	0.9 ± 0.1	R1: 1.2 ± 0.1 R2: 0.40 ± 0.02	–	0.008 ± 0.001	R1: 0.25 ± 0.01 R2: 0.43 ± 0.01	7.00 ± 0.1
$t_c = 7$ min						
Jurkat cells (Charras et al. 2006) hypo-osmotic	1.0 ± 0.1	R1: 1.2 ± 0.1 R2: 0.43 ± 0.02	–	0.012 ± 0.001	R1: 0.25 ± 0.01 R2: 0.45 ± 0.01	6.54 ± 0.1
$t_c = 12$ min						
Jurkat cells (Warren et al. 2013) hypo-osmotic	1.0 ± 0.1	R1: 1.3 ± 0.1 R2: 0.45 ± 0.02	–	0.040 ± 0.005	R1: 0.25 ± 0.01 R2: 0.45 ± 0.01	5.70 ± 0.1
$t_c = 18$ min						
Jurkat cells (Warren et al. 2013) hypo-osmotic	1.1 ± 0.1	R1: 1.3 ± 0.1 R2: 0.45 ± 0.02	–	0.050 ± 0.005	R1: 0.25 ± 0.01 R2: 0.48 ± 0.01	5.50 ± 0.1
$t_c = 23$ min						
Jurkat cells (Warren et al. 2013) hypo-osmotic	1.1 ± 0.1	R1: 1.3 ± 0.1 R2: 0.45 ± 0.02	–	0.055 ± 0.005	R1: 0.25 ± 0.01 R2: 0.50 ± 0.01	5.20 ± 0.1
$t_c = 28$ min						
Fibroblasts (Jonas et al. 2006)	30 ± 2	28 ± 1	–	0.010 ± 0.001	0.28 ± 0.01	2.72 ± 0.1
Lung cells (Alcaraz et al. 2003) A549	250 ± 5	300 ± 5	1.5 ± 0.2	–	0.28 ± 0.01	–
Lung cells (Alcaraz et al. 2003) BEAC	260 ± 5	320 ± 5	2.3 ± 0.2	–	0.27 ± 0.01	–
Muscle cells (Fabry et al. 2001)	550 ± 5	1200 ± 10	1.8 ± 0.2	–	0.22 ± 0.01	–

R1 and R2 are regime 1 and regime 2

osmotic conditions. Membrane stretching under hypo-osmotic conditions caused conformational changes of the cortical ABP. Relaxation of the cortex to stretching requires specific timeframes. The results point that longer contact times $t_c \geq 18$ min ensured structural reorganization which leads to the cortex stiffness. For $t_c \leq 7$ min structural changes are not observed. The optimal model parameters for all experimental conditions are shown in Table 2. Increase of the cortex stiffness corresponding to the contact time induces additionally energy storage and energy dissipation. Energy storage was quantified by the increase of the shear modulus G_{sC} (the reversible regular part) and the effective cortex modulus η_{effC} (the reversible anomalous part) for $t_c \geq 18$ min. The increase of η_{effC} for

$t_c \geq 18$ min is pronounced for higher angular velocities (regime 2). It is expected in the context that higher angular velocity regime leads to higher amount of energy storage and energy dissipation. Anomalous nature of the energy dissipation was quantified by the higher values of the effective modulus η_{effC} for the cortex and η_{effL} for the lipid bilayer as well as the damping coefficient α for $t_c \geq 18$ min. Higher value of the effective modulus of the cortex η_{effC} was obtained at low angular velocities (in regime 1). However, higher angular velocities induce decrease of the η_{effC} in regime 2. This indicates a shearing behavior of the cortex obtained for Jurkat cells. Values of the effective modulus of the cortex η_{effC} in regime 2 were of the same order of magnitude as obtained

Fig. 2 Storage and loss moduli as a function of angular velocity for Jurkat cells under iso-osmotic condition

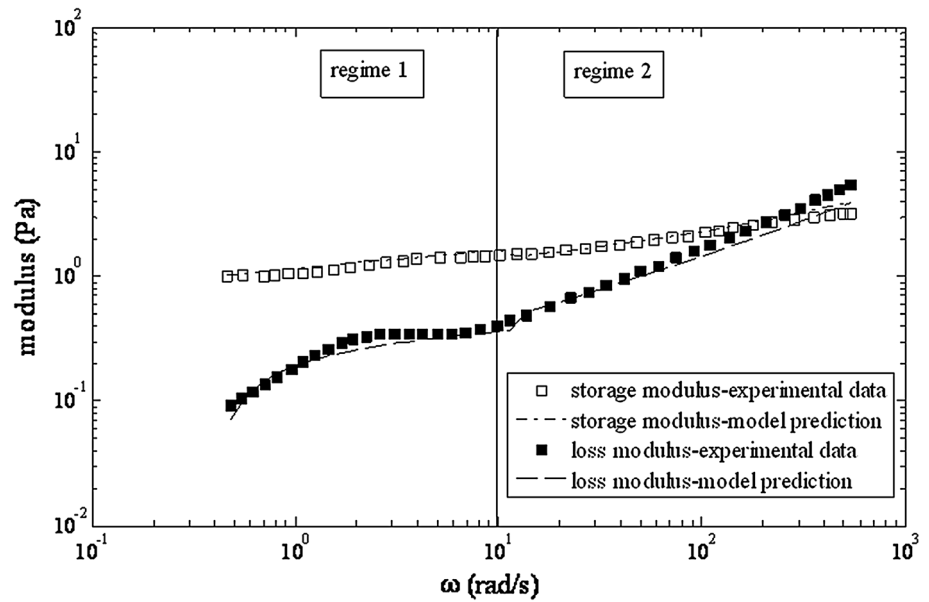
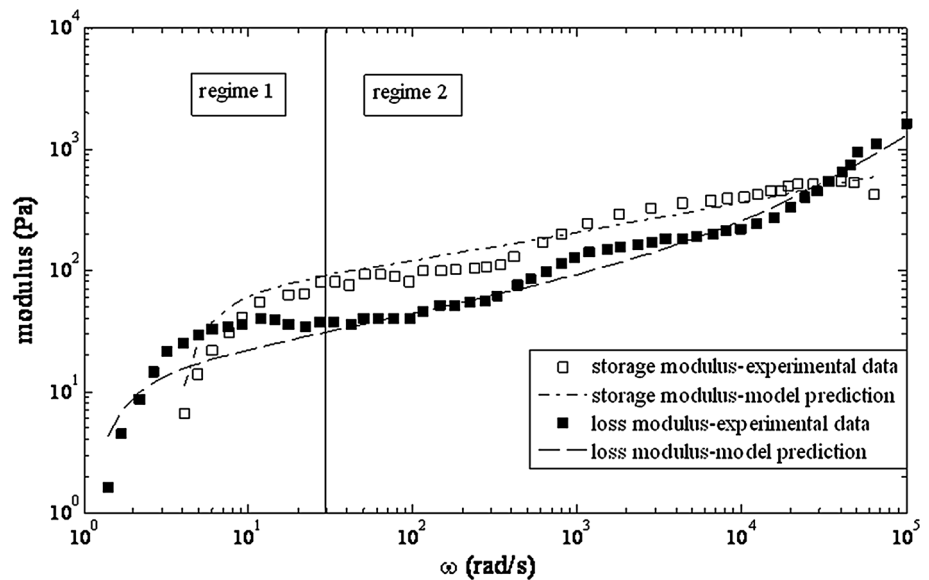


Fig. 3 Storage and loss moduli as a function of angular velocity for fibroblasts



for erythrocytes (Table 2). Higher values of the damping coefficient α were obtained in regime 2 relative to regime 1 indicating more intensive energy dissipation during the membrane structural ordering. The rearrangement times obtained for Jurkat cells were of the order of magnitude higher than that previously determined for erythrocytes (Table 2). It is in accordance with the fact that the erythrocyte spectrin-actin cortex is more mobile than the cortex of Jurkat cells. The average size of the cortex micro domains could be calculated from the value of 3D bulk shear modulus G_{sC} and the thickness of the cortex h_C . Previously calculated values of the average size of the cortex micro domains for erythrocytes vary from 3.0 to

5.3 μm (Table 2). We supposed preliminary that thickness of Jurkat cell cortex is similar as that observed for fibroblasts and equal to $\sim 0.1 \mu\text{m}$ (Bausch et al. 1998). The corresponding average size of the micro domains is $\sim 0.22 \mu\text{m}$ under iso-osmotic condition and decreases up to $\sim 0.20 \mu\text{m}$ under hypo-osmotic conditions. The result indicates that the Jurkat cell cortex is more homogeneous than the erythrocyte spectrin-actin network.

The storage and loss moduli versus angular velocity for fibroblasts reported by Jonas et al. (2006) are shown in Fig. 3. The model correlated with the experimental data with the standard deviation $SD = 0.145$ for the storage modulus and $SD = 0.194$ for the loss modulus. Higher

Fig. 4 Storage and loss moduli as a function of angular velocity for lung cells (human alveolar epithelial cells A549)

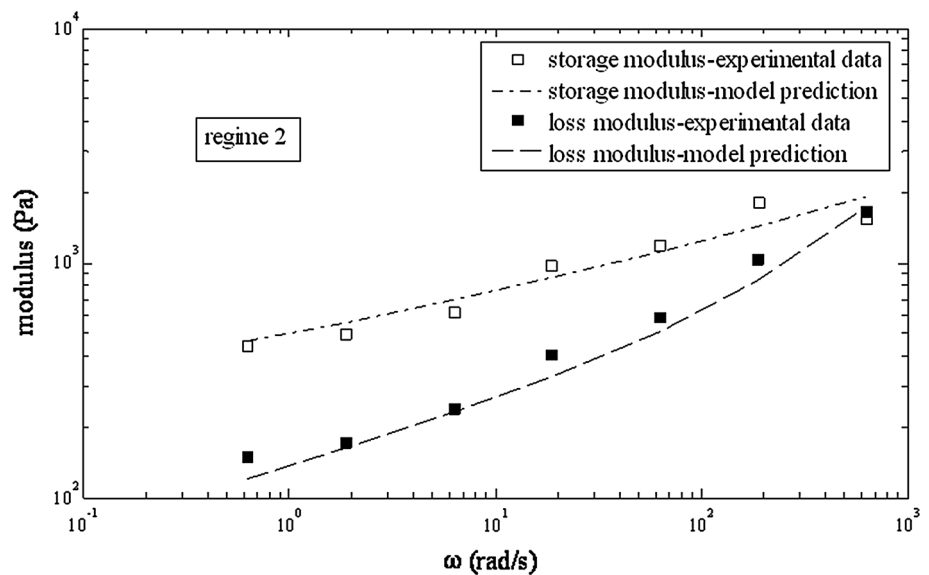
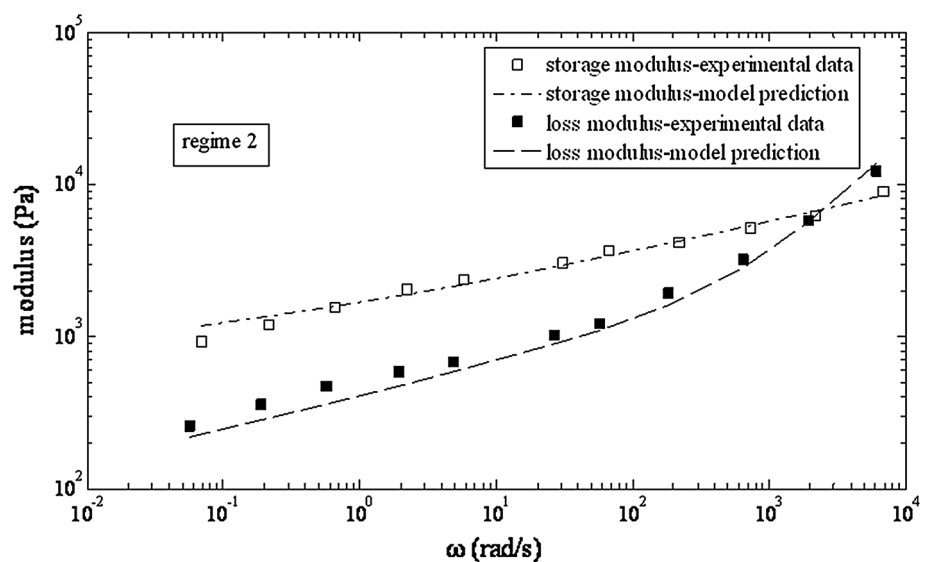


Fig. 5 Storage and loss moduli as a function of angular velocity for muscle cells



values of the storage and loss moduli for the same angular velocities were obtained for fibroblasts (Jonas et al. 2006) than for Jurkat cells (Warren et al. 2013) indicating the stiffer cortex structure. Stiffness of the fibroblast cortex was quantified by values that are 30 times higher than those of the shear modulus G_{sC} in comparison to the ones obtained for Jurkat cells. However, both cell type show ability to the cortex rearrangement at lower angular velocities (regime 1). The estimated threshold angular velocity between the regimes ω^* for fibroblasts is about $30 \frac{\text{rad}}{\text{s}}$, similar to that for erythrocytes. Rheological behavior of fibroblasts could be also described by model Eqs. 10–11 proposed for softer cell types. Unlike Jurkat cells, the effective modulus η_{effC} and the damping coefficient α were unchanged in both

regimes, indicating the stiffer cortex structure. The rearrangement times of the cortex micro domains were of the same order of magnitude as those obtained for Jurkat cells. The thickness of the fibroblasts cortex is $\sim 0.1 \mu\text{m}$ (Bausch et al. 1998). The corresponding average size of the micro domains is $\sim 36 \text{ nm}$. The result indicates that fibroblast cortex is more homogeneous than erythrocyte cortex and Jurkat cell cortex.

The storage and loss moduli versus angular velocity for lung cells: (1) human alveolar A549 and (2) bronchial epithelial cells BEAC, reported by Alcaraz et al. (2003) were considered. The experimental data for both epithelial cell types show similar functional trend. The one representative data set for A549 is shown in Fig. 4. The model

correlated with the experimental data with the standard deviation $SD = 0.0521 \pm 0.012$ for the storage modulus and $SD = 0.0852 \pm 0.006$ for the loss modulus for both cell types. Higher values of the storage and loss moduli for the same angular velocities were obtained for lung cells (Alcaraz et al. 2003) than for fibroblasts (Jonas et al. 2006) and Jurkat cells (Warren et al. 2013), indicating the stiffer cortex structure quantified by higher values of the shear modulus G_{sC} . The ability of the lung cells cortex to rearrange is not observed based on experimental data (Alcaraz et al. 2003). Their rheological behavior could be described by Eq. 12 proposed for stiffer cell types. Corresponding model parameters are shown in Table 2.

The storage and loss moduli versus angular velocity for muscle cells reported by Fabry et al. (2001) are shown in Fig. 5. The model correlated with the experimental data with the standard deviation $SD = 0.0643$ for the storage modulus and $SD = 0.0701$ for the loss modulus. The values of the storage and loss moduli were the highest for the same angular velocities in comparison to other described cell types. The ability of the muscle cortex to rearrange is not observed based on experimental data (Fabry et al. 2001). Their rheological behavior could be also described by Eq. 12. Shear modulus G_{sC} and the effective modulus η_{effC} were the highest. The value of the damping coefficient α was lower than those obtained for lung cells indicating lower ability to structural adaptation under loading conditions which is the behavior specific for solid bodies.

Conclusions

Comparison modeling analysis of the cell membrane viscoelasticity points to an anomalous nature of energy dissipation caused by coupling between the lipid bilayer and the actin cortex for various cell types: erythrocytes, Jurkat cells, fibroblasts, epithelial lung cells, and muscle cells. Experimental data indicates that softer cells such as erythrocytes, Jurkat cells, and fibroblasts show rapid non-linear increase of the storage and loss moduli at low angular velocity while the same behavior has not been observed for stiffer cells such as lung and muscle cells.

This non-linear stiffening is connected with the cortex rearrangement caused by coupling with the lipid bilayer. The cortex ability to rearrange at low angular velocities significantly depends on actin filaments mobility within the network. It is quantified by the model parameters: (1) the average size of the cortex micro domains and (2) the rearrangement time. The micro domains are connected with disorder to order phase transition of actin filaments. The average size of the cortex micro domains for erythrocytes varied from 3.0 to 5.3 μm , for Jurkat cells was $\sim 0.20\text{--}0.22 \mu\text{m}$ and for fibroblasts was $\sim 36 \text{ nm}$. Lower

size of the micro domains indicates lower actin mobility specific for the stiffer cortex structure. The rearrangement time of the cortex for Jurkat cells and fibroblasts was in the range of 2.70–7.53 s, while the rearrangement times for erythrocytes were of the order of magnitude lower.

In summary, a comparative analysis among experimental data sets and model predictions for various cell types is very important to understand general aspects of cell rheology.

Acknowledgments The authors gratefully acknowledge funding support of the Ministry of Education, Science and Technological Development of the Republic Serbia (Grants III 46001, and III 46010).

Conflict of interest The author reports no conflict of interest.

References

- Alcaraz J, Buscemi L, Grabulosa M, Trepast X, Fabry B, Farre R, Navajas D (2003) Microrheology of human lung epithelial cells measured by atomic force microscopy. *Biophys J* 84:2071–2079
- Almenar-Queralt A, Gregorio CC, Fowler VM (1999) Tropomodulin assembles early in myofibrillogenesis in chick skeletal muscle: evidence that thin filaments rearrange to form striated myofibrils. *J Cell Sci* 112:1111–1123
- Amin MS, Park YK, Lue N, Dasari RR, Badizadegan K, Feld MS, Popescu G (2007) Microrheology of red blood cell membrane using dynamics scattering microscopy. *Opt Express* 15(25):17001–17009
- Bausch AR, Ziemann F, Boulbitc AA, Jacobson K, Sackmann E (1998) Local measurements of viscoelastic parameters of adherent cell surfaces by magnetic bead microrheometry. *Biophys J* 75:2038–2049
- Borukhov I, Bruinsma RF, Gelbart WM, Liu AJ, Lubensky TC (2005) Structural polymorphism of the cytoskeleton: a model of linker-assisted filament aggregation. *PNAS* 102(10):3673–3678
- Cai X, Xing X, Cai J, Chen Q, Wu S, Huang F (2010) Connection between biomechanics and cytoskeleton structure of lymphocyte and Jurkat cells: an AFM study. *Micron* 41:257–262
- Charras GT, Hu CK, Coughlin M, Mitchison TJ (2006) Reassembly of contractile actin cortex in cell biology. *J Cell Biol* 175(3):477–490
- Dalhaimer P, Discher DE, Lubensky TC (2007) Crosslinked actin network show liquid crystal elastomeric behavior, including soft-mode elasticity. *Nature Phys* 3:354–360
- Djordjevic VD, Jaric J, Fabrz B, Fredberg JJ, Stamenovic D (2003) Fractional derivatives embody essential features of cell rheological behavior. *Ann Biomed Eng* 31:692–699
- Dustin ML, Davis SJ (2014) TCR signaling: the barrier within. *Nature Immunol* 15:136–137
- Fabry B, Maksym GN, Butler JP, Glogauer M, Navajas D, Fredberg JJ (2001) Scaling the microrheology of living cells. *Phys Rev Lett* 87(14):148102-1-4
- Feneberg W, Aepfelbacher M, Sackmann E (2004) Microviscoelasticity of the apical cell surface of human umbilical vein endothelial cells (HUVEC) within confluent monolayers. *Biophys J* 87:1338–1350
- Gov NS (2007) Less is more: removing membrane attachments stiffens the RBC cytoskeleton. *New J Phys* 9(429):1–8
- Harland CW, Bradley MJ, Parthasarathy R (2011) Retraction for “Phospholipid bilayers are viscoelastic”, by Harland CW, Bradley MJ, Parthasarathy R, which appeared in *PNAS* 2011, 107(45), pp. 19146–19150, (2010). *PNAS* 108(35):14705

- Jonas M, Chung E, Kim YH, So PTC (2006) Cytoskeletal mechanics fast fluorescence microrheology. *GEM⁴*—August 2006—MIT So Lab—FLTM, 1–3
- Kuznetsova TG, Maria N, Starodubtseva MN, Yegorenkov NI, Chizhik SA, Zhdanov RI (2007) Atomic force microscopy probing of cell elasticity. *Micron* 38:824–833
- Mangeat P, Burridge K (1984) Actin-membrane interaction in fibroblast: what proteins are involved in this association? *J Cell Biol* 99(1):95s–103s
- Mikhalyov I, Samsonov A (2011) Lipid raft detecting in membranes of live erythrocytes. *Biochem Biophys Acta* 1808:1930–1939
- Mofrad MRK, Karcher H, Kamm RD (2006) Continuum elastic or viscoelastic models for the cell. In: Mofrad MRK, Kamm RD (eds) *Cytoskeletal mechanics, models and measurement*. Cambridge University Press, New York, pp 71–84
- Pajic-Lijakovic I, Milivojevic M (2014) Modeling analysis of the lipid bilayer-cytoskeleton coupling in erythrocyte membrane. *Biomech Model Mechanobiol*. doi:[10.1007/s10237-014-0559-7](https://doi.org/10.1007/s10237-014-0559-7)
- Peng Z, Zhu Q (2013) Deformation of the erythrocyte cytoskeleton in tank treading motions. *Soft Matter* 9:7617–7627
- Podlubny I (1999) *Fractional differential equations, mathematics in science and engineering*, vol 198. Academic Press, London, p 78
- Popescu G, Park YK, Dasari RR, Badizadegan K, Feld MS (2007) Coherence properties of red blood cell membrane motion. *Phys Rev E* 76:031902-1-5
- Pradhan D, Tseng K, Cianci CD, Morrow JS (2004) Antibodies to hIA2 spectrin identify in-homogeneities in the erythrocyte membrane skeleton. *Blood Cells Mol Dis* 32:408–410
- Puig-de-Morales-Marinkovic M, Turner KT, Butler JP, Fredberg JJ, Suresh S (2007) Viscoelasticity of the human red blood cell. *Am J Physiol Cell Physiol* 293:C597–C605
- Wagh AA, Roan E, Waters CM (2008) Localized elasticity measured in epithelial cells migrating at a wound edge using atomic force microscopy. *Am J Physiol Lung Cell Mol Physiol* 295(1):L54–L60
- Wagner B, Tharmann R, Haase I, Fischer M, Bausch AR (2006) Cytoskeletal polymer networks: the molecular structure of cross-linkers determines macroscopic properties. *PNAS* 103(38):13974–13978
- Warren RL, Tassieri M, Li X, Glidle A, Paterson DJ, Carlsson A, Cooper JM (2013) Rheology at the micro-scale: new tools for bioanalysis. In: *Optical methods for inspection, characterization and imaging of biomaterials*, 13–16, Munich, Germany, Proc SPIE Vol. 8792, p. 8792141 1-13